Dalton Transactions

PAPER

View Article Online
View Journal | View Issue

Cite this: *Dalton Trans.*, 2017, **46**, 11584

Formation of unexpected silicon- and disiloxane-bridged multiferrocenyl derivatives bearing Si–O–CH=CH_2 and Si–$(CH_2)_2C(CH_3)_3$ substituents *via* cleavage of tetrahydrofuran and trapping of its ring fragments†

Sonia Bruña, [a,b] Ana Mª González-Vadillo, [a] Marta Ferrández,[a] Josefina Perles, [c] M. Merced Montero-Campillo,[d] Otilia Mó[b,d] and Isabel Cuadrado *[a,b]

The formation of a family of silicon- and siloxane-bridged multiferrocenyl derivatives carrying different functional groups attached to silicon, including $Fc_2(CH_3)_3C(CH_2)_2SiCH{=}CH_2$ (**5**), $Fc_2(CH_2{=}CH{-}O)SiCH{=}CH_2$ (**6**), $Fc_2(OH)SiCH{=}CH_2$ (**7**), $Fc_2(CH_2{=}CH{-}O)Si{-}O{-}Si(O{-}CH{=}CH_2)Fc_2$ (**8**) and $Fc_2(CH_2{=}CH{-}O)Si{-}O{-}SiFc_3$ (**9**) is described. Silyl vinyl ether molecules **6**, **8** and **9** and the heteroleptic vinylsilane **5** resulted from the competing metathesis reaction of lithioferrocene (FcLi), $CH_2{=}CH{-}OLi$ or $(CH_3)_3C(CH_2)_2Li$ with the corresponding multifunctional chlorosilane, $Cl_3SiCH{=}CH_2$ or $Cl_3Si{-}O{-}SiCl_3$. The last two organolithium species have been likely formed *in situ* by fragmentation of the tetrahydrofuran solvent. Diferrocenylvinyloxyvinylsilane **6** is noteworthy since it represents a rare example of a redox-active silyl mononomer in which two different C=C polymerisable groups are directly connected to silicon. The molecular structures of the silicon-containing multiferrocenyl species **5**, **6**, **8** and **9** have been investigated by single-crystal X-ray diffraction studies, demonstrating the capture and storage processes of two ring fragments resulting from the cleavage of cyclic THF in redox-active and stable crystalline organometallic compounds. From electrochemical studies we found that by changing the anion of the supporting electrolyte from $[PF_6]^-$ to $[B(C_6F_5)_4]^-$, the redox behaviour of tetrametallic disiloxane **8** can be switched from a poorly resolved multistep redox process to four consecutive well-separated one-electron oxidations, corresponding to the sequential oxidation of the four ferrocenyl moieties.

Received 23rd June 2017,
Accepted 21st July 2017

DOI: 10.1039/c7dt02286g

rsc.li/dalton

Introduction

Reactions with organolithium compounds are of fundamental and practical interest, particularly because of their valuable role in organic and organometallic chemistry.[1] The deprotonation reactions of organolithiums are often carried out in the presence of ethereal solvents, such as diethyl ether and tetrahydrofuran (THF), to enhance the reactivity of organometallic reagents. However, it is well-known that these polar organometallic reagents commonly decompose ethereal solvents.[1–3] In particular, THF, the most widely employed cyclic ether, is a strongly activating solvent, highly susceptible to undergo deprotonation by alkyllithium bases such as *t*-BuLi, i-PrLi and *s*-BuLi.[1–4]

Metal-induced cleavage reactions of ethers are rather complicated and, depending on the organometallic reagent and conditions, can take place in many different forms. Scheme 1 summarises an overview of the main described degradation processes of THF. Route A represents the principal pathway for decomposition of THF by strong organolithium bases RLi (R = Me, *t*-Bu, *n*-Bu) and involves the deprotonation of the α carbon, adjacent to oxygen, to generate a C–Li bond. Subsequently, the resultant 2-furyl anion undergoes a facile

[a]*Departamento de Química Inorgánica, Facultad de Ciencias, Universidad Autónoma de Madrid, Cantoblanco, 28049 Madrid, Spain. E-mail: isabel.cuadrado@uam.es*
[b]*Institute for Advanced Research in Chemical Sciences (IAdChem), Universidad Autónoma de Madrid, Spain*
[c]*Laboratorio de Difracción de Rayos X de Monocristal, Servicio Interdepartamental de Investigación (SIDI), Universidad Autónoma de Madrid, Cantoblanco, 28049 Madrid, Spain*
[d]*Departamento de Química, Facultad de Ciencias, Universidad Autónoma de Madrid, Cantoblanco, 28049 Madrid, Spain*

†Electronic supplementary information (ESI) available: Supplementary figures referenced in the text; spectroscopic, theoretical, X-ray crystallographic and CV and SWV data. CCDC 1556608–1556612. For ESI and crystallographic data in CIF or other electronic format see DOI: 10.1039/c7dt02286g

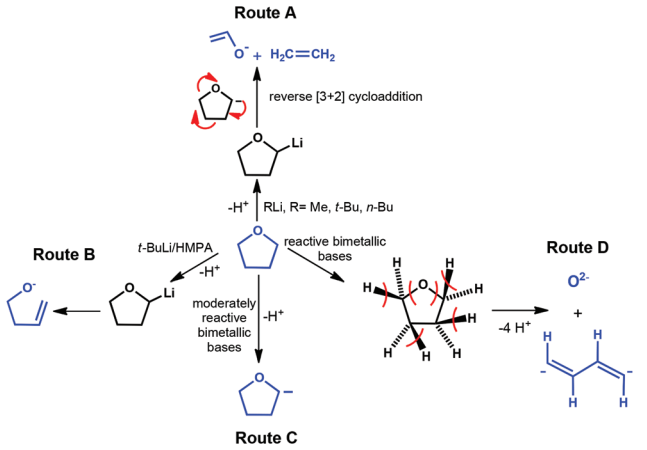

Scheme 1 Summary of the main known fragmentation reactions that the THF ring can experiment in the presence of different organometallic bases.

reverse [3 + 2] rearrangement to afford ethylene gas and the lithium enolate of acetaldehyde (CH_2=CH–OLi).[3] In rare cases, for example using a *t*-BuLi/HMPA mixture (HMPA = hexamethylphosphoric triamide ($(Me_2N)_3PO$)) (Route B) ring opening occurs but a THF ring retains the five atoms forming lithium but-3-en-1-oxide.[2] Using novel and more sophisticated synergic mixed-metal strategies, Mulvey and co-workers have observed remarkable unprecedented degradation pathways of THF. Thus, in the presence of a moderately reactive bimetallic Na/Zn base (TMEDA)Na(TMP)(CH_2SiMe_3)Zn(CH_2SiMe_3) (TMEDA = *N*,*N*,*N*′,*N*′-tetramethylethylenediamine; TMP = 2,2,6,6-tetramethylpiperidide) (Route C), α-metallation of THF occurs but the *α* deprotonated anion remains intact without any opening of the heterocyclic OC_4 ring.[5] In marked contrast to this, the more reactive heterometallic Na/Mg [(TMEDA)Na(TMP)(CH_2SiMe_3)Mg(TMP)] or Na/Mn [(TMEDA)Na(TMP)(CH_2SiMe_3)Mn(TMP)] bases promote a noteworthy cleavage of six bonds in the five-membered THF ring (Route D).[6] The two anionic fragments of the THF deconstruction shown in Route D have been trapped in separated complexes, which have been crystallographically characterised.[6]

In a related context, deprotonative metallation has proved to be of particular importance in the chemistry of ferrocene since this synthetic transformation has been frequently applied for the derivatisation of the ferrocene backbone. The reagents classically used for this purpose are organolithiums such as *n*-BuLi and *t*-BuLi.[7] Accordingly, both 1-lithioferrocene (FcLi)[8] and dimetallated 1,1′-dilithioferrocene Fe(η^5-$C_5H_4Li)_2$, ($fcLi_2$)[9] have been prepared and often used as valuable intermediates in the synthesis of new ferrocene derivatives as they readily undergo transmetallation or nucleophilic substitution reactions. In addition, recent work by Mulvey and co-workers has shown that direct multimetallation of ferrocene with mixed bimetallic synergic bases is also possible.[10] One of the most noteworthy examples of this chemistry is the 1,1′,3,3′-tetramagnesiation of ferrocene using the sodium tris(amido) magnesiate base NaMg($NiPr_2)_3$.[10b,c] In addition to promoting unique polymetallation of ferrocene, some of these bimetallic reagents are particularly useful for the functionalisation of substituted ferrocenes bearing sensitive organic functional groups such as nitriles, esters or carboxylic acids.[11–13]

Over the years, our research interest concerns the chemistry of silicon-containing multiferrocenyl compounds.[14,15] As contributions to this field, we have recently synthesised and studied Si-vinyl and Si–H functionalised triferrocenyl molecules Fc_3SiCH=CH_2 (**1**)[16] and Fc_3SiH (**2**)[17] (Fc = (η^5-C_5H_4)Fe (η^5-C_5H_5)). Triferrocenylvinylsilane **1** was prepared from 1-lithioferrocene, in turn generated by the transmetallation of 1-(tri-*n*-butylstannyl)ferrocene ($FcSnBu_3$) with *n*-BuLi, followed by quenching with the electrophile trichlorovinylsilane. In contrast, the synthesis of homoleptic hydrosilane **2** was effected in a one-pot procedure, in which 1-lithioferrocene was directly generated *in situ*, by the reaction of ferrocene and *t*-BuLi, in a 1 : 1 mixture of THF and *n*-hexane.[17] Over the course of this reaction we found that, in addition to the desired Si–H-functionalised triferrocenylsilane **2**, diferrocenyl(3,3-dimethylbutyl) silane $Fc_2(CH_3)_3C(CH_2)_2SiH$ (**3**) was unexpectedly generated. The formation of heteroleptic silicon hydride **3** is proposed to occur *via* the competitive metathesis reaction of Cl_3SiH with organolithium bases FcLi and $(CH_3)_3C(CH_2)_2Li$, which, in turn, has been formed *in situ via* the carbolithiation of ethene, generated by degradation of THF.

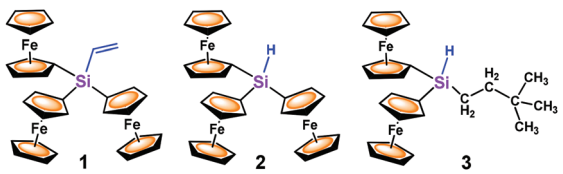

Encouraged by these results, we subsequently became interested in exploring the reaction of Cl_3SiCH=CH_2 with 1-lithioferrocene, directly generated from ferrocene and *t*-BuLi in THF, and furthermore to test the reactivity of a more complex chlorosilane, Cl_3Si–O–$SiCl_3$. In addition, to improve the yield of triferrocenylvinylsilyl **1**, the ultimate focus of this work was to obtain new functionalised ferrocenes by the capturing of molecular fragments generated from the fragmentation of cyclic THF.

Herein we report on the formation of structurally new multiferrocenyl silanes and disiloxanes, namely $Fc_2(CH_3)_3C(CH_2)_2SiCH$=$CH_2$ (**5**), $Fc_2(CH_2$=CH–O)$SiCH$=CH_2 (**6**), $Fc_2(OH)SiCH$=CH_2 (**7**), $Fc_2(CH_2$=CH–O)Si–O–Si(O–CH=$CH_2)Fc_2$ (**8**) and $Fc_2(CH_2$=CH–O)Si–O–$SiFc_3$ (**9**). These vinylsilyl compounds have been serendipitously generated from the reaction of ferrocene, *t*-BuLi and the corresponding multifunctional chlorosilane in the presence of a cyclic THF solvent. The formation of **6**, **8** and **9**, bearing the reactive silyl vinyl ether group (–Si–O–CH=CH_2), is noteworthy since it not only provides new experimental proof about the fragmentation mechanism of cyclic THF, but also points to a new potentially useful synthetic way to functionalised ferrocenes. It is interesting to

note that, among vinylsilanes, those bearing oxygen substituents at silicon are particularly useful, as these reagents consistently provide superior reactivity compared to their alkylsilyl counterparts.[18]

Results and discussion

Reaction of monolithioferrocene with $Cl_3SiCH{=}CH_2$: formation of $Fc_3SiCH{=}CH_2$ (1), $Fc_2(CH_3)_3C(CH_2)_2SiCH{=}CH_2$ (5), $Fc_2(CH_2{=}CH{-}O)SiCH{=}CH_2$ (6) and $Fc_2(OH)SiCH{=}CH_2$ (7)

Two different synthetic strategies were explored for the formation of triferrocenylvinylsilane (**1**). Both routes, A and B, are shown in Scheme 2 and involve the lithiation of ferrocene followed by the low temperature salt metathesis reaction of 1-lithioferrocene (FcLi) and the chlorosilane $Cl_3SiCH{=}CH_2$. Within these approaches, the use of pure FcLi is a key factor, in order to exclude the formation of dimetallated ferrocene, Fe$(\eta^5\text{-}C_5H_4Li)_2$, ($fcLi_2$), which could produce undesirable di-substituted- and oligo-ferrocene products. While the dilithiation of ferrocene with *n*-butyllithium in the presence of the chelating diamine TMEDA to afford $fcLi_2$ is well-established,[9] in marked contrast, the selective formation of monolithioferrocene is a very challenging synthetic task in organometallic chemistry. In our long experience, the yields of this reaction were quite variable. A convenient procedure for FcLi was reported by Guillaneux and Kagan,[8a] and involved the use of 1-(tri-*n*-butylstannyl)ferrocene as an excellent precursor of 1-lithioferrocene, leading, through reaction with suitable electrophiles, to monosubstituted ferrocenes in high yields.

Accordingly, in our first attempt to prepare **1**, with three ferrocenyl moieties attached to the vinylsilane functionality, we used a two-step synthetic procedure starting from $FcSnBu_3$ as the monolithioferrocene precursor (Scheme 2, Route A).[16] Subsequently, the transmetallation of $FcSnBu_3$ was achieved by treatment with *n*-BuLi at −78 °C, followed by quenching with $Cl_3SiCH{=}CH_2$. After removing the insoluble LiCl and subsequent purification *via* column chromatography, the target Si-vinyl-terminated **1** was isolated in high purity and reasonable yield (42%). During the purification of the reaction mixture, tetraferrocenyl disiloxane **4** was also obtained. Most likely, this initially unexpected tetrametallic compound **4** was formed under the used reaction conditions, as a result of the condensation reaction of a silanol-containing diferrocenyl molecule $Fc_2(OH)SiCH{=}CH_2$, in turn generated accidentally, either by partial hydrolysis of the starting trichlorovinylsilane or by hydrolysis of chlorodiferrocenylvinylsilane $Fc_2(Cl)SiCH{=}CH_2$, as it is shown in Scheme S1 (see the ESI†).[16] Triferrocenyl compound **1** has proven to be a particularly reactive vinylsilane and has been successfully incorporated, *via* hydrosilylation chemistry, around the surface of polyhedral octasilsesquioxane cages (POSS) and linear and cyclic siloxane scaffolds.[14c]

With the aim to improve the yield of vinylsilane **1**, to reduce the number of reaction steps, and mainly, to check whether new functionalised ferrocenes were formed, in an alternative approach 1-lithioferrocene was directly generated *in situ* in a single synthetic step, from the reaction between ferrocene and *t*-BuLi in a 1 : 1 mixture of THF and *n*-hexane at −10 °C (Scheme 2, Route B). Subsequently, without isolation of the pyrophoric solid FcLi, a THF solution of trichlorovinylsilane was added dropwise to the reaction mixture cooled at −20 °C.

After the separation of the solid LiCl and appropriate workup of the crude product, the ^{1}H NMR spectrum of the reaction mixture (see the ESI, Fig. S1†) exhibited the signals of targeted compound **1** and the apparition of new cyclopentadienyl resonances due to unknown monosubstituted ferrocenyl species. Thus, two complex multiplets centred at δ 1.00–1.50 ppm characteristic of linked CH_2 groups, and a very intense singlet at δ 0.95 ppm, clearly attributable to the protons of decoupled methyl units were observed. In addition, informative resonances in the vinyl region also appeared. These key NMR spectroscopic data motivated us to isolate the unknown compounds and properly investigate their origins and molecular structures.

The purification of the crude reaction product by careful column chromatography on silica gel allowed us to separate a first band containing unreacted ferrocene, followed by other

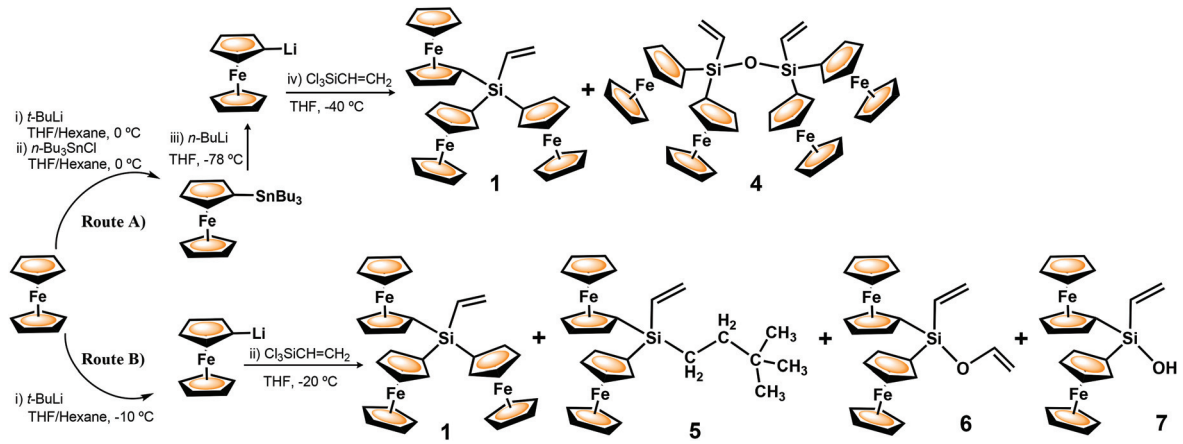

Scheme 2 Alternative routes for the reaction of 1-lithioferrocene and trichlorovinylsilane.

orange bands. The first one, eluted with *n*-hexane/CH_2Cl_2 (10 : 1), contained a yellow-orange crystalline compound which was isolated in 6% yield, in high purity, and unequivocally identified as diferrocenyl(3,3-dimethylbutyl)vinylsilane (**5**). This heteroleptic silane supports the resonances observed at δ 1.00–1.50 and 0.95 ppm in the ^{1}H NMR spectrum of the reaction mixture (see the ESI, Fig. S1†). The second band, eluted with *n*-hexane/CH_2Cl_2 (10 : 2) was found to contain a mixture of the expected compound **1** and a new mysterious vinylsilane **6**. Unfortunately, both compounds have very similar physical properties and have been therefore particularly difficult to separate. Luckily after repeated column chromatographies and several recrystallization processes using different mixtures of *n*-hexane/CH_2Cl_2, we achieved the separation and isolation of pure samples of the targeted vinylsilane **1** (in 65% yield) and the new ferrocenyl species **6** (in 9% yield). On the basis of multinuclear NMR spectroscopy, mass spectrometry and X-ray studies (see below) the unknown compound was unequivocally identified as $Fc_2(CH_2{=}CH{-}O)SiCH{=}CH_2$ (**6**), an interesting molecule bearing two ferrocenyl moieties and two types of C=C double bonds (one directly connected to silicon, and the other one to oxygen), thus explaining the striking ^{1}H NMR resonances observed in the vinyl region in the spectrum of the reaction mixture.

The origin of the initially unexpected vinylsilanes $Fc_2(CH_3)_3C(CH_2)_2SiCH{=}CH_2$ (**5**) and $Fc_2(CH_2{=}CH{-}O)SiCH{=}CH_2$ (**6**) is certainly noteworthy and deserves an explanation. Their formation can be rationalised by the sequence of processes outlined in Scheme 3, and presumably involves the THF cleavage. As already mentioned in the introduction (Scheme 1), the main pathway for the THF degradation by RLi reagents first comprises the deprotonation at the carbon α to oxygen. Then, the resultant 2-furyl anion undergoes a reverse [3 + 2] cycloaddition to generate ethylene and the lithium enolate of acetaldehyde. Therefore, probably, compound **6** carrying both a vinyloxy and a vinyl group has been formed under the used reaction conditions, as a result of the competing salt-metathesis reaction of the organolithium reagents FcLi and $CH_2{=}CH{-}OLi$ with $Cl_3SiCH{=}CH_2$. Meanwhile, diferrocenyl compound **5** is likely formed as a result of the competing metathesis reaction of FcLi and $(CH_3)_3C(CH_2)_2Li$ with $Cl_3SiCH{=}CH_2$. As observed during the formation of heteroleptic hydrosilane **3**,[17] the only plausible source of the lithiated reagent $(CH_3)_3C(CH_2)_2Li$ is the intermolecular carbolithiation of ethylene arising from the decomposition of THF (Scheme 3).[1–3]

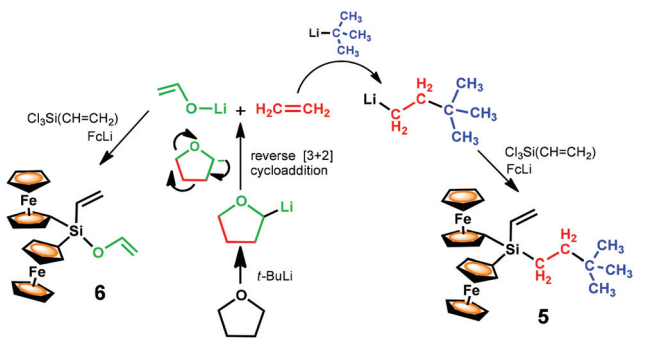

Scheme 3 Pathway for the degradation of THF and reactions that presumably occur in the system THF/*t*-BuLi/FcLi/$Cl_3SiCH{=}CH_2$.

When comparing the two synthetic procedures used to prepare **1** it can be concluded that Route B resulted more efficient and less complicated than the approach using $FcSnBu_3$ as a starting material and that, in addition, newly interesting products, **5** and **6**, have been formed. The reaction of FcLi with $Cl_3SiCH{=}CH_2$ following Route B (Scheme 2) was repeatedly performed and in all the cases compounds **1**, **5** and **6** were obtained. In addition, in some reactions, diferrocenylvinylsilanol (**7**) was also isolated. The formation of compound **7** provides significant evidence to affirm that disiloxane **4**, obtained by Route A, was generated as a result of the condensation reaction of silanol-containing intermediates, as we previously proposed (see the ESI, Scheme S1†).[16] Compound **7** was purified by column chromatography and was isolated as an air stable, yellow-orangish crystalline solid in 5% yield.

It must be emphasised that compounds **6** and **7** carry two different reactive and polymerisable groups, allowing them to participate in different chemical transformations. In addition, the polar vinyl ether reactive group present in **6** is an attractive functionalisation due to its versatile and rich reactivity.[18]

Once separated, the new multiferrocenyl vinylsilanes **5–7** were thoroughly characterised by elemental analysis, multinuclear NMR spectroscopy, IR and MALDI-TOF mass spectrometry. In addition to the ferrocenyl resonances, the ^{1}H NMR spectra of **5–7** show three double doublets in the expected integrated ratios, which are consistent with the vinyl AMX system. Furthermore, the ^{1}H NMR spectrum of **5** shows the peculiar pattern for the $-(CH_2)_2C(CH_3)_3$ group, a singlet at δ 0.94 ppm corresponding to the nine protons of the three decoupled methyl groups, and two complex multiplets centred at δ 1.02 and 1.44 ppm characteristic of the $-CH_2-CH_2-$ unit. The $-O-CH{=}CH_2$ group of **6** appears as a double doublet at δ 6.59 and two doublets, one centred at δ 4.58 while the other one cannot be observed because it is overlapped with the C_5H_5 resonance at δ 4.16 ppm. This last signal could be identified performing a $\{^1H{-}^{13}C\}$ HMQC experiment (see the ESI, Fig. S9†), as the carbon resonance of the $-O-CH{=}CH_2$ unit correlates, not only with the multiplet at δ 4.58 ppm, but also with the other that is under the C_5H_5 resonance at δ 4.16 ppm. Meanwhile, the spectrum of compound **7** exhibits a singlet at δ 2.15 ppm, distinctive of the OH group.

Besides the characteristic carbon signals of the ferrocenyl units and of the vinyl groups (at 133 and 137 ppm), the ^{13}C NMR spectrum of **5** shows the resonances of the 3,3-dimethylbutyl group. Thus, the CH_2 carbons appear at δ 9.0 and 38.3 ppm, the CH_3 at δ 28.9 ppm, and the *ipso*-carbon at δ 31.3 ppm. In the spectrum of compound **6** two resonances of the $-O-CH{=}CH_2$ group appear at δ 94.2 and 146.3 ppm. The ^{29}Si NMR spectrum displays a single resonance at δ −17.0 ppm (for **1**), δ −12.1 ppm (for **5**), δ −7.8 ppm (for **6**), and at δ −8.9 ppm (for **7**). Therefore, the replacement of a ferrocenyl

moiety by a 3,3-dimethylbutyl shifts the silicon signals downfield. These resonances are even more deshielded in the spectra of compounds **6** and **7**, due to the electronic influence of the –OCH=CH_2 and –OH groups.

Reaction of monolithioferrocene with hexachlorodisiloxane: formation of $Fc_2(CH_2{=}CH{-}O)Si{-}O{-}Si(O{-}CH{=}CH_2)Fc_2$ (8), $Fc_2(CH_2{=}CH{-}O)Si{-}O{-}SiFc_3$ (9) and $Fc_3Si{-}O{-}SiFc_3$ (10)

Encouraged by the results described above and with the idea to increase the members of the multiferrocenyl family supported by Si–O–Si bridges, our efforts were next directed toward the synthesis of a disiloxane maximally functionalised with as many ferrocenyl units as chemically possible. Thus, we sought to prepare the hexaferrocenyldisiloxane molecule **10** shown in Scheme 4. To this end, monolithioferrocene was generated by treating ferrocene with *t*-BuLi, in a 1 : 1 mixture of THF and *n*-hexane at −10 °C. Subsequently, FcLi was reacted with hexachlorodisiloxane ($Cl_3Si{-}O{-}SiCl_3$) at −20 °C and the reaction mixture was purified by column chromatography. To our surprise, the tetrametallic compound $Fc_2(CH_2{=}CH{-}O)Si{-}O{-}Si(O{-}CH{=}CH_2)Fc_2$ (**8**) was isolated as the major reaction product (29% yield). Compound **8** is a disiloxane functionalised with four ferrocenyl units and two vinyloxy reactive groups, which was isolated as an orange, crystalline and air stable solid. It is interesting to observe that, in addition to the peak of **8** at *m*/*z* 898.1, the MALDI-TOF mass spectrum of the reaction mixture (see Fig. 1) exhibits two peaks at *m*/*z* 1040.0 and 1182.0, thus confirming the formation of the targeted hexaferrocenyldisiloxane **10** and of an asymmetric disiloxane molecule, $Fc_2(CH_2{=}CH{-}O)Si{-}O{-}SiFc_3$ (**9**), also shown in Scheme 4.

Unfortunately, significant amounts of pure samples of multiferrocenyl disiloxanes **9** and **10** could not be isolated, so far, due to their similar solubility properties. However, their existence is fully supported by the MALDI-TOF mass spectrometric study and, in the case of disiloxane **9** by X-ray diffraction analysis (see below).

On the basis of the formation of silylated acetaldehyde species **6**, it seems reasonable to assume that disiloxanes **8** and **9** were formed as a result of the competing metathesis reactions of FcLi and CH_2=CH–OLi to react with the hexachlorodisiloxane, according to Scheme 5.

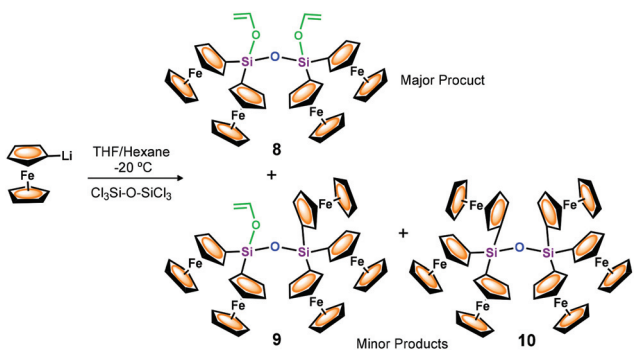

Scheme 4 Synthesis of polyferrocenes **8–10** with disiloxane bridges.

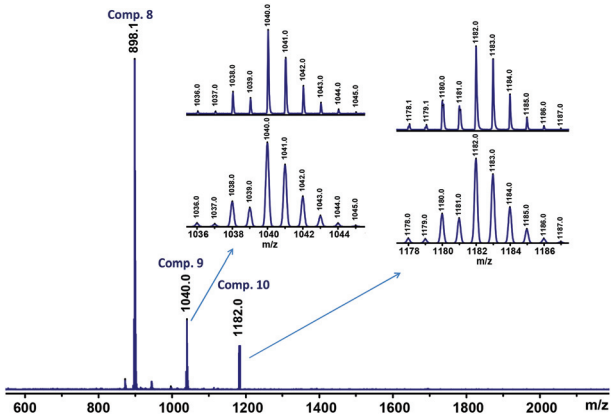

Fig. 1 MALDI-TOF mass spectrum of the reaction mixture of disiloxanes **8–10**. The insets show the experimental (top) and calculated (bottom) isotopic patterns for compounds **9** and **10**.

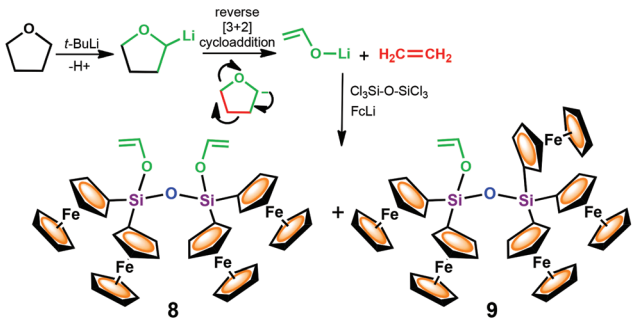

Scheme 5 Reactions that presumably occur in the system THF/*t*-BuLi/FcLi/$Cl_3Si{-}O{-}SiCl_3$.

As can be observed, the reaction between FcLi and $Cl_3Si{-}O{-}SiCl_3$ fails to give the desired hexaferrocenyl **10** in preparative amounts, which might be due to the steric repulsion of the six ferrocenyl moieties in close contact across the siloxane bond. Therefore, it is very likely that the difficulty entailed in effectively bonding six ferrocenyl units to the Si–O–Si bridge facilitates, as an alternative reaction route, the incorporation of the less bulky vinyloxy group.

We have to note that neither disiloxane **8** nor vinylsilanes **5** and **6** are accessible by conventional organosilicon chemistry methods, illustrating again the synthetic potential of THF-cleavage reactions.

Multinuclear NMR (^{1}H, ^{13}C and ^{29}Si) analyses of the new disiloxane **8** were consistent with the proposed structure. Thus, the protons of the –O–CH=CH_2 groups appear in the ^{1}H NMR spectrum at 6.82 ppm (double doublet) and at δ 4.68 and 4.26 ppm (doublets). The ^{29}Si NMR of **8** presents a single resonance at δ −27.7 ppm, in good agreement with values found for other ferrocenyl disiloxanes.[14]

Crystal structures of compounds 5–9

The ultimate confirmation that the molecular fragments generated from the cleavage of the THF ring have been certainly

captured in crystalline redox-active ferrocenyl compounds was achieved by single-crystal X-ray diffraction analysis of silanes **5** and **6** and disiloxanes **8** and **9**.

Diffraction-grade single crystals were obtained by crystallisation at 4 °C in *n*-hexane/CH_2Cl_2 (10 : 2) for **5**, at room temperature in CH_2Cl_2 for **6** and **7** and at 4 °C in *n*-hexane/CH_2Cl_2 (10 : 3) for **8** and **9**. The resulting structures are shown in Fig. 2 and 3, and complete structural information is collected in the ESI.† The three bimetallic silanes **5**–**7** and the pentametallic disiloxane **9** crystallise in the triclinic space group $P\bar{1}$ with one (**6**, **7** and **9**) or two (**5**) molecules per asymmetric unit, while tetrametallic disiloxane **8** belongs to the monoclinic $P2_1/n$ space group. The two crystallographic independent molecules in the asymmetric unit cell of **5** (**5**A and **5**B) are shown in Fig. 2 (top); they differ only slightly in their bond lengths and angles.

In both molecules, the two ferrocenyl groups attached to the silicon atoms are disposed in a nearly perpendicular arrangement. The cyclopentadienyl rings in **5** are parallel (maximum deviation 2.22° for the Cps attached to Fe2) and essentially eclipsed in three of the ferrocenyl moieties, while

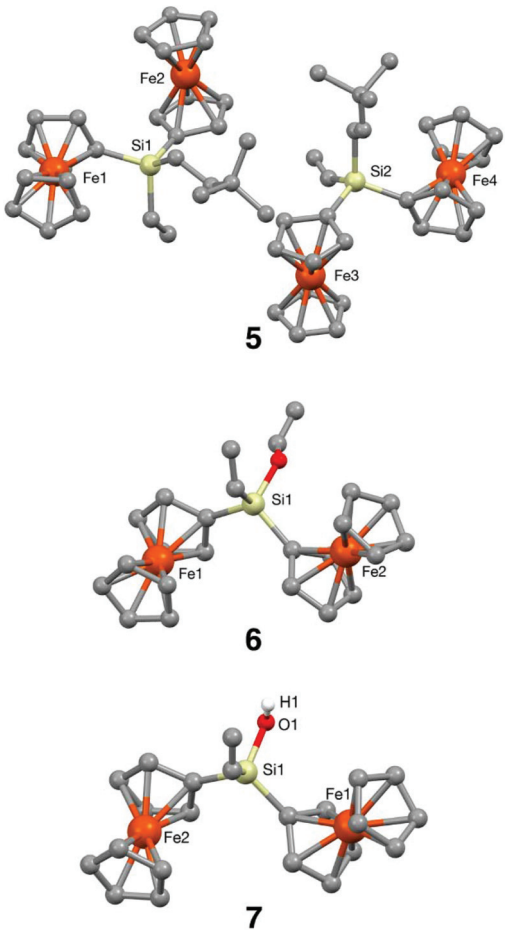

Fig. 2 Molecular structures of silanes **5**–**7** with selected atoms labelled. Hydrogen atoms (except the hydroxylic one) have been removed for clarity.

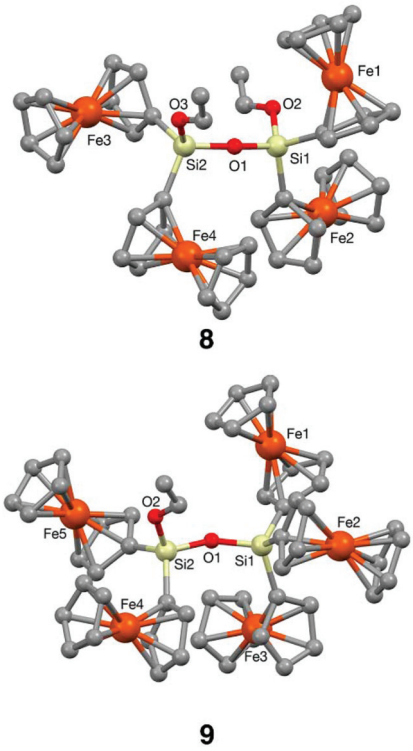

Fig. 3 Molecular structures of disiloxanes **8** and **9** with selected atoms labelled. Hydrogen atoms have been removed for clarity.

in the fourth one (the one comprising Fe3) they are completely staggered. The intramolecular distances between Fe atoms are 6.0556(8) Å (Fe1–Fe2) and 6.1853(8) Å (Fe3–Fe4). The supramolecular arrangement is achieved by van der Waals forces, giving rise to four-molecule rings.

In the bifunctional compound **6** (Fig. 2, middle), the cyclopentadienyl rings are also essentially parallel (maximum deviation 2.81° in the ferrocene containing Fe1) and eclipsed. Iron atoms are separated by 6.0857(6) Å and no relevant supramolecular interactions have been found.

In diferrocenylsilanol **7** (Fig. 2, bottom) the disposition of the Fc units is very similar to the one observed in **6**, with the cyclopentadienyl rings parallel (maximum deviation 2.36° in the Fc with Fe2) and eclipsed, presenting an intramolecular distance between Fe atoms of 6.1174(6) Å. However, in this structure hydrogen bonds between the pairs of molecules are responsible for the formation of dimeric units (see the ESI, Fig. S31† and Table S12†). This is in agreement with the IR data, where a ν(OH) band at 3413 cm^{-1} was observed, which corresponds to Si–OH groups linked by hydrogen bonds. The fact that the two diferrocenylsilanols **6** and **7** show an almost identical molecular conformation and very similar packing patterns (see the ESI, Fig. S32†) regardless of the difference in supramolecular interactions, proves the important role that the shape and size of these molecules play in their arrangement in the crystal state. In this case, the smaller substituent in **7** together with the existence of hydrogen bonds, lead to a closer packing of the molecules involved in the supramolecu-

lar interactions, which in turn yields a denser crystal (calculated density values are 1.473 for **6** and 1.526 Mg cm^{-3} for **7**).

In disiloxanes **8** and **9** (Fig. 3) the ferrocenyl units are placed as distant as possible from each other in order to avoid steric congestion around the silicon atoms, and the Si–O–CH=CH$_2$ groups are arranged in zig-zag chains. These two disiloxanes show a bent arrangement of the disiloxane linkage, with Si–O–Si angles of 160.0(1)° for **8** and 152.9(2)° for **9**. The Fe atoms of the ferrocenyl substituents attached to the same silicon centre are separated by 5.9037(5) and 6.1052(5) Å (**8**) and by 5.444(1), 6.501(1) and 6.077(1) Å (**9**). Meanwhile, the iron centres of the ferrocenyl units attached to different silicon atoms (see the ESI, Table S11†) are separated by larger distances, ranging from 6.3853(7) to 8.4029(6) Å (for **8**) and from 6.501(1) to 9.327(1) Å (for **9**).

In all of the crystal structures **5–9**, the silicon atoms are nearly tetrahedral with C–Si–C (for **5–9**), C–Si–O (for **6–9**) and O–Si–O (for **8** and **9**) bond angles close to 109° (see the ESI, Fig. Table S13†) and similar to the ones obtained for **1**.[9]

Electrochemistry and electronic structure calculations

The redox properties of **5–8**, featuring ferrocenyl moieties linked by a silicon atom and/or a disiloxane bridge, are also of considerable interest as these molecules display multielectron redox chemistry.[19] The electrochemical behaviour was investigated by cyclic voltammetry (CV) and square wave voltammetry (SWV), using CH_2Cl_2 as a non-nucleophilic solvent, and tetra-*n*-butylammonium hexafluorophosphate ([*n*-Bu$_4$N][PF$_6$]) or tetra-*n*-butylammonium tetrakis(pentafluorophenyl)borate ([*n*-Bu$_4$N][B(C$_6$F$_5$)$_4$]) as supporting electrolytes containing anions of different coordinating ability. Geiger and co-workers have performed remarkable studies on the perfluoroarylborate anion [B(C$_6$F$_5$)$_4$]$^-$ and have ascribed the improvements observed in the oxidative electrochemical processes of organometallic compounds to its intrinsically low ion-pairing strengths and nucleophilicities, and to the increased solubility of its salts in lower polarity solvents as compared to classical electrolytes such as [PF$_6$]$^-$, [ClO$_4$]$^-$ and [BF$_4$]$^-$.[20]

Diferrocenyl silanes **5–7** constitute the simplest molecules described here and they are structurally related to the homoleptic vinylsilane **1** and heteroleptic diferrocenyl-vinylsilane Fc$_2$(CH$_3$)SiCH=CH$_2$ previously investigated by us.[14d,16] They are constituted by a vinyl reactive group and two identical ferrocenyl units, linked together by a silicon bridge, and they vary in the nature of the non-electroactive –O–CH=CH$_2$, –(CH$_2$)$_2$C(CH$_3$)$_3$ or –OH substituent (R in Fig. 4 top). As expected, this leads to qualitatively similar voltammetric responses which differ only slightly in the half-wave potentials $E_{1/2}$, reflecting the different electronic influences of the fourth substituent (R) at silicon. As representative examples, Fig. 4(A–D) present the CV and SWV responses obtained for **5**. In CH_2Cl_2 using either the traditional [PF$_6$]$^-$ or the non-coordinating [B(C$_6$F$_5$)$_4$]$^-$ electrolyte anion, the electrochemical oxidation of **5** takes place in two well-resolved voltammetric waves, which correspond to the sequential oxidation of the two ferrocenyl moieties, giving the ferrocenium species **5**$^+$ and **5**$^{2+}$. Experimentally measured

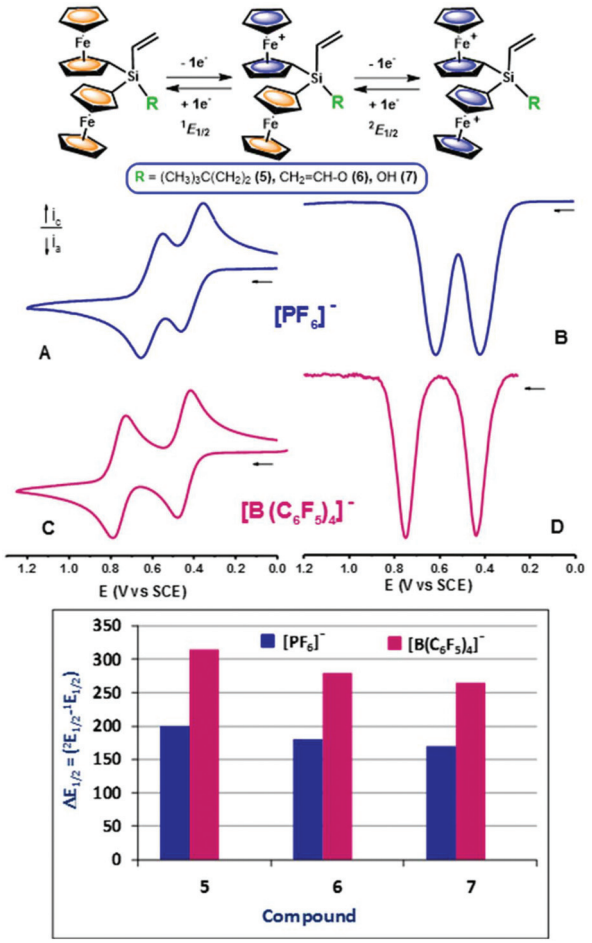

Fig. 4 Top: Redox processes experimented by diferrocenylvinylsilanes **5–7**. Voltammetric responses, on a Pt electrode, of **5**: (A) and (B) recorded in CH_2Cl_2 containing 0.1 M [*n*-Bu$_4$N][PF$_6$]; (C) and (D) recorded in CH_2Cl_2 containing 0.1 M [*n*-Bu$_4$N][B(C$_6$F$_5$)$_4$]. CVs are at a scan rate of 0.1 V s^{-1}. Bottom: $\Delta E_{1/2}$ values for the two successive oxidations of **5–7** measured in CH_2Cl_2 in the presence of the weakly coordinating [B(C$_6$F$_5$)$_4$]$^-$ (red) or the traditional [PF$_6$]$^-$ (blue) supporting electrolyte anions.

potential values are $^1E_{1/2}$ = 0.420 and $^2E_{1/2}$ = 0.620 V ($\Delta E_{1/2}$ = $^2E_{1/2}$ – $^1E_{1/2}$ = 200 mV) (in [*n*-Bu$_4$N][PF$_6$]) and $^1E_{1/2}$ = 0.422 and $^2E_{1/2}$ = 0.737 V ($\Delta E_{1/2}$ = 315 mV) (in [*n*-Bu$_4$N][B(C$_6$F$_5$)$_4$]). Similarly, the CVs and SWVs of **6** and **7** also showed two successive clearly defined ferrocene-based oxidation waves separated by $\Delta E_{1/2}$ = 180 and 170 mV (in [*n*-Bu$_4$N][PF$_6$]) and by $\Delta E_{1/2}$ = 280 and 264 mV (in [*n*-Bu$_4$N][B(C$_6$F$_5$)$_4$]). These findings suggest the existence of appreciable iron–iron interactions between the two neighboring ferrocenyl units linked to the silicon atom. The structurally related linear and cyclic oligo- and polyferrocenylsilanes, having similar silicon-bridged ferrocenyl moieties, have been extensively studied by Manners[21] and Pannell[22] and exhibit electronic communication between adjacent iron centres.[23]

For redox-active multimetallic compounds, the magnitude of the separation between the half-wave potentials ($\Delta E_{1/2}$) of two redox sites has usually been taken as a measure of

electronic interactions between metal centres. However, one should be extremely careful when using electrochemical data since voltammetric separations are influenced by the effects of the solvent/supporting electrolyte media, which can modify the electrostatic interactions in polycationic species.

The graphical comparison of $\Delta E_{1/2}$ values shown in the bottom of Fig. 4 is also representative of the changes in the redox splitting between the first and second redox events observed for diferrocenylsilanes **5–7** when changing the anion of the supporting electrolyte from nucleophilic $[PF_6]^-$ to weakly coordinating fluoroarylborate anion. The fact that in the three compounds the low ion-pairing supporting electrolyte $[n\text{-}Bu_4N][B(C_6F_5)_4]$ increases the separation of the two one-electron oxidations suggests that the through-space interaction is also significant. In addition, this figure shows that the incorporation of $-(CH_2)_2C(CH_3)_3$ substituent in the bridging silicon of diferrocenyl **5** results in an enlarged peak separation, which can be attributed to more effective intermetallic communication between the two ferrocenyl units.

The determination of redox potentials for the successive oxidations of **5–7** allowed us to estimate the comproportionation constant, K_c, relative to the equilibrium $[Fe^{II}\text{–}Fe^{II}] + [Fe^{III}\text{–}Fe^{III}] \leftrightarrow [Fe^{II}\text{–}Fe^{III}]$.[24] The wave splitting ($\Delta E_{1/2}$) between the first and second oxidations measured in the weakly coordinating supporting electrolyte $[n\text{-}Bu_4N][B(C_6F_5)_4]$ and the K_c are both indicative of the thermodynamic stability of the mixed valence state of these molecules relative to other redox systems.[25] The resulting values of K_c are 211.15×10^3 (for **5**), 54.07×10^3 (for **6**) and 29.01×10^3 (for **7**), calculated from $\Delta E_{1/2}$ electrochemical values, indicating that intermetallic interaction exists in the partially oxidised multiferrocenyl compounds **5–7**.[19b,26]

Many times, a strong electronic communication between active redox centres is allowed by the presence of unsaturated or aromatic units in the bridge. This is nicely reflected in the shape of the HOMO, which involves the bridge, as a sign of delocalisation of the charge. However, neither **6–7**[27] nor **5** (see Fig. 5A) present a HOMO orbital involving the silicon bridges, something not surprising in class II mixed-valence compounds. When dealing with these systems in a vacuum, *i.e.*, looking strictly at the chemical structure, weak non-covalent interactions in the van der Waals range are already observed between the substituents in the silicon bridge and the ferrocenyl units, as evidenced by the NCI (Non Covalent Interaction) analysis represented by green isosurfaces in Fig. 5B. Undoubtedly, the solvent/electrolyte medium plays a very important role on modulating and reinforcing these interactions between centres, as previously observed in the voltammetric measurements. Upon oxidation, the corresponding SOMO orbital occupies the next ferrocenyl unit to be oxidised (Fig. 5A). We obtain a vertical ionisation potential value of 6.08 eV for **5**, in agreement with previous values for compounds **6** and **7** (6.16 and 6.08 eV).[27] The calculated UV-Vis spectrum of **5** in CH_2Cl_2 along with the different orbital contributions to each transition is provided in Fig. S35 and Table S14 (see the ESI†).

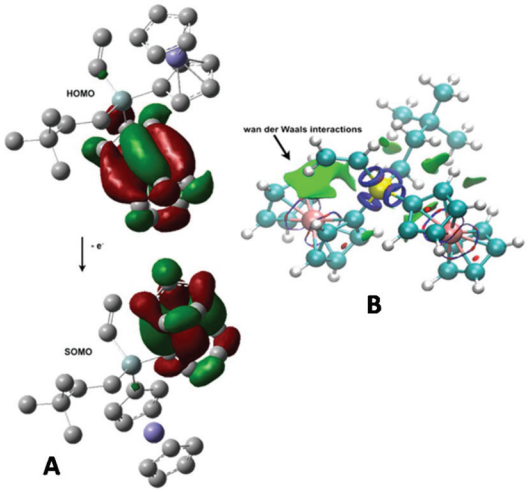

Fig. 5 (A): HOMO and SOMO orbitals of compound **5** at the BPW91/6-31+G(d) level of theory. (B): NCI analysis carried out by means of the NCIPLOT program. Blue and red colors denote strong attractive and repulsive interactions, respectively, whereas green color indicates interactions in the van der Waals range.

In addition, electronic structure calculations show that compound **5** presents a different variation of the partial charge of both Fe atoms (0.119 and 0.190 a.u.) after the first oxidation, in agreement with the electrochemical results. This compound exhibits slightly larger iron charge variations on their response to oxidation with respect to values reported for compounds **6** and **7** at the same level of theory.[27] Accordingly, spin densities on iron atoms in the radical species present values of 0.699 and 0.398 a.u.

We have also explored the electrochemical oxidation of **8** since the four ferrocenyl redox moieties linked by the Si–O–Si bridge provide an excellent opportunity to study multi-step electron-transfer processes. As shown in Fig. 6, the CV of **8** in CH_2Cl_2/0.1 M $[n\text{-}Bu_4N][PF_6]$ is considerably more complex than that of the diferrocenyl compounds **5–7**, as it exhibits a sequence of several overlapped, and poorly resolved, waves (from about +0.45 to +0.85 V *vs.* SCE), thereby preventing a detailed analysis of the successive individual oxidations. The more anodic wave is not a diffusion-controlled process and a sharp cathodic stripping wave is observed on the return sweep. This indicates that for disiloxane **8**, a change in solubility accompanies the change in the oxidation state, very likely due to the rapid precipitation of the hexafluorophosphate salt $[\mathbf{8}^{4+}][PF_6]_4$ on the electrode surface. On the reverse scan, this tetraoxidised cation is redissolved as it is reduced. Such electrochemical phenomena are well known for multi-ferrocenyl compounds,[28] where solubility problems and follow-up reactions result in deviations from ideality when using the traditional nucleophilic electrolyte anion $[PF_6]^-$ in low-polarity solvents.

By using $[n\text{-}Bu_4N][B(C_6F_5)_4]$ as an electrolyte, we hoped to accurately investigate the multistep electron-transfer processes of tetrametallic **8**, because the weakly coordinating $[B(C_6F_5)_4]^-$

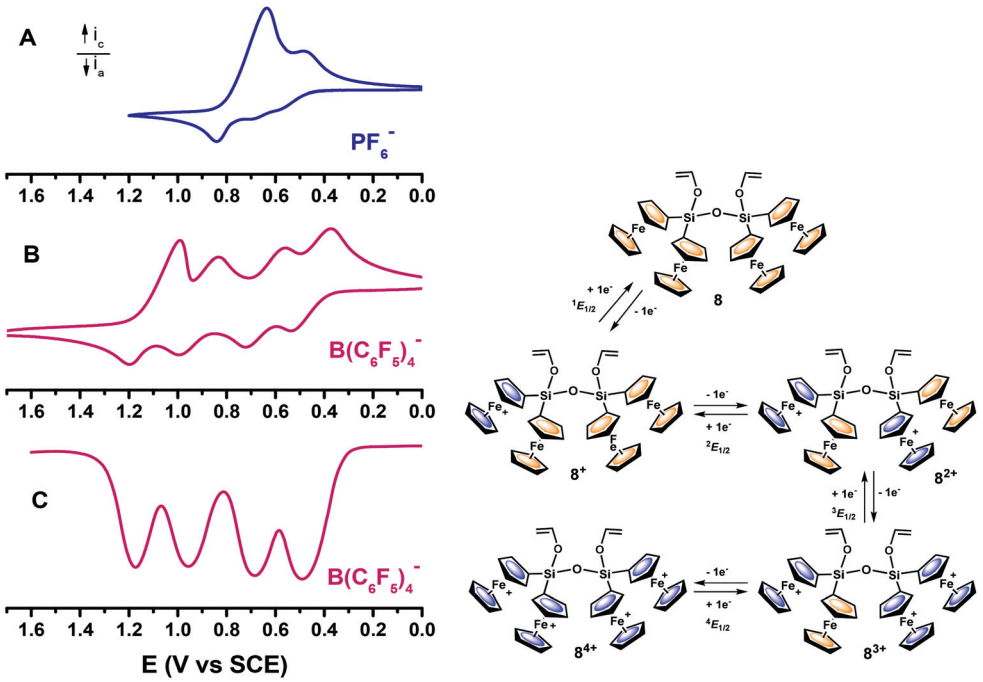

Fig. 6 Cyclic and SWV responses, on a platinum electrode of tetrametallic **8**, recorded in CH_2Cl_2 containing 0.1 M [*n*-Bu_4N][PF_6] (A) or 0.1 M [*n*-Bu_4N][$B(C_6F_5)_4$] (B and C) as supporting electrolytes. CVs at a scan rate of 0.1 V s^{-1}.

anion is extremely effective in solubilising positively charged species produced in anodic processes.

Thus, Fig. 6 compares the CV of **8** in CH_2Cl_2/[NBu_4][PF_6] with those of the same molecule in CH_2Cl_2 with 0.1 M [*n*-Bu_4N][$B(C_6F_5)_4$], and shows the striking improvement observed for the anodic reaction of this tetrametallic disiloxane. With $[B(C_6F_5)_4]^-$ the adsorption effects on the working electrode were minimised, which indicates an increase in solubility of the tetracationic species $\mathbf{8}^{4+}$ in this solvent/electrolyte medium. In addition, in agreement with the results reported by Geiger and coworkers, as compared to the small inorganic $[PF_6]^-$ anion, the $[B(C_6F_5)_4]^-$ electrolyte anion has a lower coordinating power and restrains ion pairing, allowing the development of interactions between the four metallocene units in **8**, which are electrostatic in nature, that is, mostly through-space interactions. This results in the observation of four well-resolved one-electron oxidation waves, at different potentials, for each of the four ferrocenyl moieties. Likewise, SWV of **8** measured in CH_2Cl_2/[*n*-Bu_4N][$B(C_6F_5)_4$] (Fig. 6C) also shows four well-separated waves. The height peak of the two more anodic waves is somewhat smaller than that of the first two waves. This effect has been previously observed in ferrocenyl[29] and fulvalenediyl multimetallic compounds[30] and can be taken as a qualitative indication that the last one-electron transfers are slightly slower than that of the first two oxidations.[31]

The mechanism for the electrochemical oxidation of this tetrametallic disiloxane is shown in Fig. 6 and involves a first oxidation (at $^1E_{1/2}$ = +0.484 V *vs.* SCE) corresponding to the generation of monocationic species $\mathbf{8}^+$. At a higher potential ($^2E_{1/2}$ = +0.696 V) a second electron is removed from a ferrocenyl moiety attached to the neighbouring silicon atom, at the other end of the Si–O–Si bridge, yielding the dicationic species $\mathbf{8}^{2+}$. The potential separation between the second and third redox processes, $\Delta E_{1/2} = {}^3E_{1/2} - {}^2E_{1/2}$ = 256 mV, is larger than $^2E_{1/2} - {}^1E_{1/2}$ = 212 mV and $^4E_{1/2} - {}^3E_{1/2}$ = 228 mV, implying that the third oxidation (at $^3E_{1/2}$ = +0.952 V) occurs at one of the two remaining ferrocenyl moieties, the adjacent to the last oxidised ferrocenyl subunit.[14e,16] The final oxidation of the last neutral ferrocenyl centre is the most difficult one and takes place at more anodic potential ($^4E_{1/2}$ = +1.180 V), giving the tetracationic species $\mathbf{8}^{4+}$. The considerable spread of the four oxidations in disiloxane **8** suggests appreciable intermetallic interactions between the Si- and Si–O–Si-bridged ferrocenyl moieties.[14e,16] The observed shifts of the oxidation potential values for the $\mathbf{8}/\mathbf{8}^+/\mathbf{8}^{2+}/\mathbf{8}^{3+}/\mathbf{8}^{4+}$ couples (see Fig. 6) when going from $[PF_6]^-$ to $[B(C_6F_5)_4]^-$ media are consistent with a considerable decrease in the ion pairing of the Fe^{III} centres with the weakly coordinating fluoroarylborate anion as the ferrocenyl moieties are progressively oxidised.

Experimental section

General considerations

General procedures and equipment. All reactions and compound manipulations were performed under an oxygen- and moisture-free Ar atmosphere using standard Schlenk techniques. THF was distilled over sodium/benzophenone under argon before use. *n*-Hexane and dichloromethane were dried by standard procedures over appropriate drying agents and dis-

tilled under argon, immediately prior to use. Ferrocene (Sigma-Aldrich) was purified by sublimation prior to use. Trichlorovinylsilane, hexachlorodisiloxane and *t*-butyllithium (1.7 M solution in *n*-pentane) (Sigma-Aldrich) were used as received. Silica gel (70–230 mesh) (Sigma-Aldrich) was used for column chromatography purifications. Infrared spectra were recorded on a PerkinElmer 100 FT-IR spectrometer. Elemental analyses were performed in a LECO CHNS-932 elemental analyzer, equipped with a MX5 Mettler Toledo microbalance. All NMR spectra were recorded on a Bruker Avance 300 MHz spectrometer. Chemical shifts were reported in parts per million (δ) with reference to $CDCl_3$ residual solvent resonances for ^1H (δ 7.26 ppm) and ^{13}C (δ 77.2 ppm). ^{29}Si NMR resonances were recorded with inverse-gated proton decoupling in order to minimize nuclear Overhauser effects and were referenced externally to tetramethylsilane. MALDI-TOF mass spectra were recorded using a Bruker-Ultraflex III TOF/TOF mass spectrometer equipped with a nitrogen laser emitting at 337 nm. The dichloromethane solutions of the matrix (*trans*-2-[3-(4-*tert*-butylphenyl)-2-methyl-2-propenylidene]malonitrile (DCTB), 10 mg mL^{-1}) and dichloromethane solutions of the corresponding compound (1 mg mL^{-1}) were mixed in the ratio 20 : 5. Then, 0.5–1 μL of the mixture was deposited on the target plate using the dried droplet method. The positive ion and the reflectron mode were used for these analyses.

Electrochemical measurements. Cyclic voltammetry (CV) and square wave voltammetry (SWV) experiments were recorded on a Bioanalytical Systems BAS CV-50 W potentiostat. CH_2Cl_2 and CH_3CN (SDS, spectrograde) were freshly distilled from calcium hydride under Ar. The supporting electrolytes used were tetra-*n*-butylammonium hexafluorophosphate (Alfa-Aesar), which was purified by recrystallisation from ethanol and dried in a vacuum at 60 °C, and tetra-*n*-butylammonium tetrakis(pentafluorophenyl)borate, which was synthesised as described in the literature,[32] by metathesis of [*n*-Bu_4N]Br with Li[$B(C_6F_5)_4$]·(*n*OEt_2) (Boulder Scientific Company) in methanol and recrystallised twice from CH_2Cl_2/hexane. The supporting electrolyte concentration was 0.1 M. A conventional three-electrode cell connected to an atmosphere of prepurified nitrogen was used. The counter electrode was a coiled Pt wire, and the reference electrode was a BAS saturated calomel electrode (SCE). All cyclic voltammetric experiments were performed using a platinum-disk working electrode (A = 0.020 cm^2) (BAS). The working electrode was polished on a Buehler polishing cloth with Metadi II diamond paste for about 3 min followed by sonication in absolute ethanol, rinsed thoroughly with purified water and acetone, and allowed to dry. Under our conditions, the ferrocene redox couple $[FeCp_2]^{0/+}$ is +0.462, and the decamethylferrocene redox couple $[FeCp^*_2]^{0/+}$ is −0.056 V *vs.* SCE in CH_2Cl_2/0.1 M [*n*-Bu_4N][PF_6]. Solutions were, typically, 10^{-3} M in the redox-active species and were purged with nitrogen and kept under an inert atmosphere throughout the measurements. No IR compensation was used. SWV was performed using frequencies of 10 Hz.

X-ray crystal structure determination. Suitable orange crystals of compounds **5–9** were coated with mineral oil and mounted on Mitegen MicroMounts. The samples were transferred to a Bruker D8 KAPPA series II with an APEX II area-detector system equipped with graphite monochromated Mo Kα radiation (λ = 0.71073 Å). Full details of the data collection and refinement can be found in the ESI.† The substantial redundancy in data allows empirical absorption corrections (SADABS)[33] to be applied using multiple measurements of symmetry-equivalent reflections. Raw intensity data frames were integrated with the SAINT program,[34] which also applied corrections for Lorentz and polarization effects. The Bruker SHELXTL Software Package was used for space group determination, structure solution, and refinement.[35] The space group determination was based on a check of the Laue symmetry and systematic absences were confirmed using the structure solution. The structures were solved by direct methods (SHELXS-97), completed with different Fourier syntheses, and refined with full-matrix least-squares using SHELXS-97 minimizing $\omega(F_o^2 - F_c^2)^2$.[36,37] Weighted R factors (R_w) and all goodness of fit S are based on F^2; conventional R factors (R) are based on F. All non-hydrogen atoms were refined with anisotropic displacement parameters. The hydrogen atoms were calculated geometrically and allowed to ride on their parent carbon or oxygen atoms with fixed isotropic U. All scattering factors and anomalous dispersion factors are contained in the SHELXTL 6.10 program library. The crystal structures of compounds **5–9** have been deposited at the Cambridge Crystallographic Data Centre with deposition numbers CCDC 1556608–1556612.†

Computational details. Electronic structure calculations were carried out with the Gaussian09 program.[38] Structures were fully optimized at the BPW91/6-31+G(d) level of theory.[39] Vibrational normal modes from harmonic frequency calculations allowed ensuring that all structures are minima of the potential energy surface. NCIPLOT program was used to analyse NCI (non-covalent interactions) in compound **5**.[40] This analysis shows which regions of the space present low reduced density gradient (RDG) values, a dimensionless quantity that assumes very small values for NCI regions. Non-covalent interactions are characterized by both low RDG and low electron density values. Also, the sign of eigenvalue λ_2 of the Laplacian of the density helps to distinguish between attractive ($\lambda_2 < 0$) and repulsive ($\lambda_2 > 0$) weak interactions. According to this, attractive regions appear in blue colour in three-dimensional NCI representations, whereas green surfaces denote interactions within the van der Waals range. Red colour stands for repulsive interactions. QTAIM (Quantum Theory of Atoms in Molecules) allows to analyse the molecular space from the topology of the density point of view. In particular, interacting atoms are connected through paths containing bond critical points (BCPs).[41] Density values at BCPs are a way of describing the strength of the interaction when comparing the same pair of atoms in different molecular environments. The sign of the Laplacian at the BCPs also allows classifying bonds as ionic or covalent. Closed-shell interactions as those in Fig. S43† are characterized by positive values.

Synthesis

Reaction of FcLi with $Cl_3SiCH{=}CH_2$: synthesis of $Fc_3Si{-}CH{=}CH_2$ (1), $Fc_2(CH_3)_3C(CH_2)_2SiCH{=}CH_2$ (5), $Fc_2(CH_2{=}CH{-}O)SiCH{=}CH_2$ (6) and $Fc_2(OH)SiCH{=}CH_2$ (7). 15 g of sublimed ferrocene (80.6 mmol) was dissolved in a mixture of 100 mL of dry THF and 100 mL of dry *n*-hexane, under argon at room temperature, and then cooled to −10 °C. To this stirred system, a 1.7 M solution of *t*-BuLi in *n*-pentane (72.0 mL, 121.0 mmol) was added dropwise. The mixture was stirred for another 30 min and cooled to −20 °C before a solution of $Cl_3SiCH{=}CH_2$ (3.2 mL, 24.2 mmol) in 15 mL of dry THF was added dropwise. The solution was allowed to warm to room temperature and was stirred overnight. The mixture was filtered, treated with *n*-hexane, and then filtered once again to remove the LiCl byproduct. Solvent removal yielded a red-orange oily product, which was purified by column chromatography on silica gel (6 cm × 10 cm) using *n*-hexane as an eluent. A first band containing unreacted ferrocene was eluted, and subsequently, a second orange band was obtained with *n*-hexane/CH_2Cl_2 (10 : 1). Solvent removal afforded the reaction side product **5**, which was obtained as an analytically pure, air-stable, yellow-orangish crystalline solid. Subsequently, on eluting with *n*-hexane/CH_2Cl_2 (10 : 2) a third major band was collected. Solvent removal afforded a mixture of two compounds (**1** and **6**). This mixture was subjected to a second column chromatography on silica gel (6 cm × 16 cm). A first band was eluted with *n*-hexane/CH_2Cl_2 (10 : 2) and solvent removal afforded compound **1** as an analytically pure, air-stable, orange crystalline solid. The other fractions of this column were again mixtures of compounds **1** and **6**. After several columns and recrystallisations in *n*-hexane/CH_2Cl_2, compound **6** was finally isolated as an analytically pure, air-stable, orange crystalline solid. In some of the repeated reactions, a final fraction was obtained from the first column chromatography, eluted with CH_2Cl_2. After the appropriate solvent removal process, compound **7** was obtained as a pure, air-stable, light orange crystalline solid.

*Data for **1**.* Yield: 9.59 g (65%). ^{1}H NMR ($CDCl_3$, 300 MHz, ppm): δ 4.05 (s, 15H, C_5H_5), 4.25, 4.39 (m, 12H, C_5H_4), 6.08 (dd, ^3J = 20.2 Hz, ^2J = 4.0 Hz, 1H, CH=CH_{trans}H$_{cis}$), 6.25 (dd, ^3J = 14.7 Hz, ^2J = 4.0 Hz, 1H, CH=CH$_{trans}H_{cis}$), 6.69 (dd, ^3J = 20.2 Hz, ^3J = 14.7 Hz, 1H, CH=CH$_2$). ^{13}C{^{1}H} NMR ($CDCl_3$, 75 MHz, ppm): δ 68.7 (C_5H_5), 70.8, 74.0 (C_5H_4), 132.2 (CH=CH$_2$), 136.4 (CH=CH$_2$). ^{29}Si {^{1}H} NMR ($CDCl_3$, 59 MHz, ppm): δ −17.0 (*Si*Fc). IR (KBr, cm^{-1}): ν(C=C) 1163, ν(Si–C) 820. MS (MALDI-TOF): *m*/*z* 610.1 [M$^+$]. Anal. calcd for $C_{32}H_{30}Fe_3Si$: C, 62.95; H, 4.96. Found: C, 62.68; H, 4.98.

*Data for **5**.* Yield: 0.74 g (6%). ^{1}H NMR ($CDCl_3$, 300 MHz, ppm): δ 0.94 (s, 9H, CH_3), 1.02, 1.44 (m, 4H –CH_2–), 4.10 (s, 10H, C_5H_5), 4.15, 4.37 (m, 8H, C_5H_4), 5.83 (dd, ^3J = 20.3 Hz, ^2J = 4.0 Hz, 1H, CH=CH_{trans}H$_{cis}$), 6.13 (dd, ^3J = 14.7 Hz, ^2J = 4.0 Hz, 1H, CH=CH$_{trans}H_{cis}$), 6.46 (dd, ^3J = 20.3 Hz, ^3J = 14.7 Hz, 1H, CH=CH$_2$). ^{13}C{^{1}H} NMR ($CDCl_3$, 75 MHz, ppm): δ 9.0 (Si–CH$_2$), 28.9 (CH$_3$), 31.3 (C–CH$_3$), 38.3 (CH$_2$–C), 68.4 (C_5H_5), 68.5 (*ipso*-Fc), 70.76, 70.78, 73.7, 73.8 (C_5H_4), 133.1 (CH=CH$_2$), 136.9 (CH=CH$_2$). ^{29}Si {^{1}H} NMR ($CDCl_3$, 59 MHz, ppm): δ −12.1 (*Si*Fc). IR (KBr, cm^{-1}): ν(C–C) 2950, ν(C=C) 1162, ν(Si–C) 819. MS (MALDI-TOF): *m*/*z* 510.2 [M$^+$]. Anal. calcd for $C_{28}H_{34}Fe_2Si$: C, 65.87; H, 6.71. Found: C, 65.59; H, 6.85.

*Data for **6**.* Yield: 1.02 g (9%). ^{1}H NMR ($CDCl_3$, 300 MHz, ppm): δ 4.16 (s, 10H, C_5H_5), 4.16 (d, ^3J = 5.7 Hz, 1H, O–CH=CH$_{trans}$ H_{cis}), 4.25, 4.29, 4.42 (m, 8H, C_5H_4), 4.58 (d, ^3J = 13.5 Hz, 1H, O–CH=CH_{trans} H$_{cis}$), 6.11 (dd, ^3J = 20.0 Hz, ^2J = 4.2 Hz, 1H, CH=CH_{trans}H$_{cis}$), 6.28 (dd, ^3J = 14.9 Hz, ^2J = 4.2 Hz, 1H, CH=CH$_{trans}H_{cis}$), 6.46 (dd, ^3J = 20.0 Hz, ^3J = 14.9 Hz, 1H, CH=CH$_2$), 6.59 (dd, ^3J = 13.5 Hz, ^3J = 5.7 Hz, 1H, O–CH=CH$_2$). ^{13}C{^{1}H} NMR ($CDCl_3$, 75 MHz, ppm): δ 68.5 (*ipso*-Fc), 68.7 (C_5H_5), 71.3, 71.4, 73.7, 73.8 (C_5H_4), 94.2 (O–CH=CH$_2$), 134.3 (CH=CH$_2$), 135.6 (CH=CH$_2$), 146.3 (O–CH=CH$_2$). ^{29}Si {^{1}H} NMR ($CDCl_3$, 59 MHz, ppm): δ −7.8 (*Si*Fc). IR (KBr, cm^{-1}): ν(C=C) 1633, 1167, ν(Si–C) 824. MS (MALDI-TOF): *m*/*z* 468.1 [M$^+$]. Anal. calcd for $C_{24}H_{24}Fe_2SiO$: C, 61.53; H, 5.17. Found: C, 61.36; H, 5.05.

*Data for **7**.* Yield: 0.53 g (5%). ^{1}H NMR ($CDCl_3$, 300 MHz, ppm): δ 2.15 (s, 1H, OH), 4.17 (s, 10H, C_5H_5), 4.26, 4.29, 4.42 (m, 8H, C_5H_4), 6.11 (dd, ^3J = 20.2 Hz, ^2J = 4.1 Hz, 1H, CH=CH_{trans}H$_{cis}$), 6.23 (dd, ^3J = 15.0 Hz, ^2J = 4.1 Hz, 1H, CH=CH$_{trans}H_{cis}$), 6.51 (dd, ^3J = 20.2 Hz, ^3J = 15.0 Hz, 1H, CH=CH$_2$). ^{13}C{^{1}H} NMR ($CDCl_3$, 75 MHz, ppm): δ 67.8 (*ipso*-Fc), 68.5 (C_5H_5), 71.2, 71.3, 73.4, 73.5 (C_5H_4), 134.0 (CH=CH$_2$), 136.3 (CH=CH$_2$). ^{29}Si {^{1}H} NMR ($CDCl_3$, 59 MHz, ppm): δ −8.9 (*Si*Fc). IR (KBr, cm^{-1}): ν(O–H) 3604, 3413, ν(C=C) 1166, ν(Si–C) 822. MS (MALDI-TOF): *m*/*z* 442.1 [M$^+$]. Anal. calcd for $C_{22}H_{22}Fe_2SiO$: C, 59.73; H, 5.02. Found: C, 59.60; H, 5.15.

Reaction of FcLi with $Cl_3Si{-}O{-}SiCl_3$. Formation of $Fc_2(CH_2{=}CH{-}O)Si{-}O{-}Si(O{-}CH{=}CH_2)Fc_2$ (8), $Fc_2(CH_2{=}CH{-}O)Si{-}O{-}SiFc_3$ (9) and $Fc_3Si{-}O{-}SiFc_3$ (10). Following the same procedure as the one described for the previous reaction, sublimed ferrocene (4.5 g, 24.2 mmol) was dissolved in 30 mL of dry THF and 30 mL of dry *n*-hexane and treated with a solution of $Cl_3Si{-}O{-}SiCl_3$ (0.69 mL, 3.6 mmol) in 7 mL of THF. The red-orange oily product obtained after appropriate treatment was purified by column chromatography on silica gel (3 cm × 11 cm). Unreacted ferrocene was firstly eluted with *n*-hexane and, subsequently, a second orange band was obtained with *n*-hexane/CH_2Cl_2 (10 : 3). Solvent removal afforded disiloxane **8** as an analytically pure, air-stable, yellow-orangish crystalline solid. Subsequently, on eluting with different *n*-hexane/CH_2Cl_2 mixtures, diverse bands were collected. After MALDI-TOF analysis, these fractions were found to correspond to a mixture of compounds **9** and **10**, impossible to isolate in quantitative yields.

*Data for **8**.* Yield: 0.94 g (29%). ^{1}H NMR ($CDCl_3$, 300 MHz, ppm): δ 4.16 (s, 20H, C_5H_5), 4.26 (d, ^3J = 5.8 Hz, 1H, O–CH=CH$_{trans}$ H_{cis}), 4.29, 4.36, 4.40 (m, 16H, C_5H_4), 4.68 (d, ^3J = 13.5 Hz, 1H, O–CH=CH_{trans} H$_{cis}$), 6.82 (dd, ^3J = 13.5 Hz, ^3J = 5.8 Hz, 1H, O–CH=CH$_2$). ^{13}C{^{1}H} NMR ($CDCl_3$, 75 MHz, ppm): δ 65.8 (*ipso*-Fc), 68.8 (C_5H_5), 71.1, 71.2, 73.6, 73.8 (C_5H_4), 94.6 (O–CH=CH$_2$), 145.6 (O–CH=CH$_2$). ^{29}Si{^{1}H} NMR ($CDCl_3$, 59 MHz, ppm): δ −27.7 (*Si*Fc). IR (KBr, cm^{-1}): ν(C=C) 1636, 1171, ν(Si–O–Si) 1075, ν(Si–C) 815. MS (MALDI-TOF): *m*/*z* 898.1

[M^+]. Anal. calcd for $C_{44}H_{42}Fe_4Si_2O_3$: C, 58.80; H, 4.71. Found: C, 58.95; H, 4.63.

Conclusions

In this work, we have successfully isolated and characterised several silicon- and siloxane-bridged multiferrocenyl compounds bearing different reactive groups in the solid and solution states. We propose that species $Fc_2(CH_3)_3C(CH_2)_2SiCH{=}CH_2$ (**5**), $Fc_2(CH_2{=}CH{-}O)SiCH{=}CH_2$ (**6**), $Fc_2(CH_2{=}CH{-}O)Si{-}O{-}Si(O{-}CH{=}CH_2)Fc_2$ (**8**) and $Fc_2(CH_2{=}CH{-}O)Si{-}O{-}SiFc_3$ (**9**) have resulted from the competing salt-metathesis reactions of the corresponding chlorosilanes ($Cl_3SiCH{=}CH_2$ or $Cl_3Si{-}O{-}SiCl_3$) with lithioferrocene and the organolithium reagents $CH_2{=}CH{-}OLi$ or $(CH_3)_3C(CH_2)_2Li$ which, in turn, have been generated *in situ* by degradation of THF. Multiferrocenyl species **6**, **8** and **9** are noteworthy since, for the first time, a $CH_2{=}CH{-}O^-$ fragment resulting from the cleavage of the THF ring has been entrapped and stored in very stable and redox-active compounds, which have been crystallographically characterised. To the best of our knowledge, these compounds are the first redox-active molecules containing a reactive silyl vinyl ether group. In addition, biferrocenyl **6**, carrying both a vinyl and a vinyloxy group, is also of interest since it represents the first, and so far the only example of an electroactive silyl mononomer with two different reactive polymerisable groups.

Electrochemical studies reveal that, in both electrolyte systems containing either the traditional $[PF_6]^-$ or the weakly coordinating $[B(C_6F_5)_4]^-$ anion, the silicon-bridged diferrocenylvinyl compounds **5–7** undergo two well-separated reversible one-electron oxidations, indicating intermetallic interactions between the ferrocenyl moieties. The introduction of the 3,3-dimethylbutyl group in the silicon bridge of **5** seems to increase the metal–metal interaction with respect to that of the structurally related diferrocenyl systems **6** and **7**. In addition, tetraferrocenyl disiloxane **8** displays an interesting redox behaviour that can be switched from a poorly unresolved multistep redox process, to four consecutive, clearly defined, one-electron oxidations by changing the anion of the supporting electrolyte from $[PF_6]^-$ to the weak nucleophilic and ion-pairing $[B(C_6F_5)_4]^-$ anion. Future studies will focus on studying the reactivity of **6**, **7** and **8** as redox-active bifunctional silyl monomers.

Acknowledgements

The authors are grateful to the Spanish Ministerio de Economía y Competitividad (MINECO) (projects CTQ2012-30728 and CTQ2015-63997-C2-1-P) for the generous support of this work. M. M. M.-C. and O. M. thank the STSM COST Action CM1204 and the Project FOTOCARBON-CM S2013/MIT-2841 of the Comunidad Autónoma de Madrid. Computational time at Centro de Computación Científica (CCC) of Universidad Autónoma de Madrid is acknowledged.

References

1 (*a*) M. Schlosser, in *Organometallics in Synthesis: A Manual*, ed. M. Schlosser, John Wiley & Sons Ltd, Chichester, 2nd edn, 2002, ch. 1, pp. 1–352; (*b*) J. Clayden, *Organolithiums: Selectivity for Synthesis*, Pergamon, Elsevier, Oxford, 2002, ch. 7, pp. 273–280.
2 J. Clayden and S. A. Yasin, *New J. Chem.*, 2002, **26**, 191–192.
3 R. B. Bates, L. M. Kroposki and D. E. Potter, *J. Org. Chem.*, 1972, **37**, 560–562.
4 P. Stanetty and M. D. J. Mihovilovic, *Org. Chem.*, 1997, **62**, 1514–1515.
5 A. R. Kennedy, J. Klett, R. E. Mulvey and D. S. Wright, *Science*, 2009, **326**, 706–708.
6 R. E. Mulvey, V. L. Blair, W. Clegg, A. R. Kennedy, J. Klett and L. Russo, *Nat. Chem.*, 2010, **2**, 588–591.
7 *Ferrocenes: Ligands, Materials and Biomolecules*, ed. P. Štěpnička, John Wiley & Sons Ltd, West Sussex, England, 2008.
8 (*a*) D. Guillaneux and H. B. Kagan, *J. Org. Chem.*, 1995, **60**, 2502–2505; (*b*) B. Bildstein, M. Malaun, H. Kopacka, K. Wurst, M. Mitterböck, K.-H. Ongania, G. Opromolla and P. Zanello, *Organometallics*, 1999, **18**, 4325–4336; (*c*) R. Sander and U. T. Mueller-Westherhoff, *J. Organomet. Chem.*, 1996, **512**, 219–224.
9 (*a*) M. D. Rausch and D. J. Ciappenelli, *J. Organomet. Chem.*, 1967, **10**, 127–136; (*b*) J. J. Bishop, A. Davison, M. L. Katcher, D. W. Lichtenberg, R. E. Merrill and J. C. Smart, *J. Organomet. Chem.*, 1971, **27**, 241–249; (*c*) R. F. Kovar, M. D. Rausch and H. Rosenberg, *Organomet. Chem. Synth.*, 1970/1971, **1**, 173; (*d*) D. A. Rider, K. A. Cavicchi, N. K. Power-Billard, T. P. Russell and I. Manners, *Macromolecules*, 2005, **38**, 6931–6938.
10 (*a*) K. W. Henderson, A. R. Kennedy, R. E. Mulvey, C. T. O'Hara and R. B. Rowlings, *Chem. Commun.*, 2001, 1678–1679; (*b*) W. Clegg, K. W. Henderson, A. R. Kennedy, R. E. Mulvey, C. T. O'Hara, R. B. Rowlings and D. M. Tooke, *Angew. Chem., Int. Ed.*, 2001, **40**, 3902–3905; (*c*) P. C. Andrikopoulos, D. R. Armstrong, W. Clegg, C. J. Gilfillan, E. Hevia, A. R. Kennedy, R. E. Mulvey, C. T. O'Hara, J. A. Parkinson and D. M. Tooke, *J. Am. Chem. Soc.*, 2004, **126**, 11612–11620; (*d*) W. Clegg, E. Crosbie, S. H. Dale-Black, E. Hevia, G. W. Honeyman, A. R. Kennedy, R. E. Mulvey, D. L. Ramsay and S. D. Robertson, *Organometallics*, 2015, **34**, 2580–2589.
11 E. Hevia, A. R. Kennedy and M. D. McCall, *Dalton Trans.*, 2012, **41**, 98–103.
12 G. Dayaker, A. Sreeshailam, F. Chevallier, T. Roisnel, P. R. Krishna and F. Mongin, *Chem. Commun.*, 2010, **46**, 2862–2864.
13 A. H. Stoll, P. Mayer and P. Knochel, *Organometallics*, 2007, **26**, 6694–6697.
14 (*a*) S. Bruña, A. M. González-Vadillo, D. Nieto, C. J. Pastor and I. Cuadrado, *Macromolecules*, 2012, **45**, 781–779; (*b*) M. Zamora, S. Bruña, B. Alonso and I. Cuadrado, *Macromolecules*, 2011, **44**, 7994–8007; (*c*) S. Bruña, S. D. Nieto,

A. M. González-Vadillo, J. Perles and I. Cuadrado, *Organometallics*, 2012, **31**, 3248–3258; (*d*) I. Cuadrado, C. M. Casado, B. Alonso, M. Morán, J. Losada and V. Belsky, *J. Am. Chem. Soc.*, 1997, **119**, 7613–7614; (*e*) S. Bruña, A. F. Garrido-Castro, J. Perles, M. M. Montero-Campillo, O. Mó, A. E. Kaifer and I. Cuadrado, *Organometallics*, 2016, **35**, 3507–3519; (*f*) I. Cuadrado, in *Silicon-Containing Dendritic Polymers*, ed. P. R. Dvornic and M. J. Owen, Springer, Germany, 2009, vol. 2, ch. 8, pp. 141–196.

15 For interesting examples of multiferrocenyl compounds see for instance: (*a*) L. Xu, Y.-X. Wang, L.-J. Chen and H.-B. Yang, *Chem. Soc. Rev.*, 2015, **44**, 2148–2167; (*b*) J.-K. Ou-Yang, L.-J. Chen, L. Xu, C.-H. Wang and H.-B. Yang, *Chim. Chem. Lett.*, 2013, **14**, 471–474; (*c*) Q.-J. Li, G.-Z. Zhao, L.-J. Chen, H. Tan, C.-H. Wang, D.-X. Wang, D. A. Lehman, D. C. Muddiman and H.-B. Yang, *Organometallics*, 2012, **31**, 7241–7247; (*d*) G.-Z. Zhao, Q.-J. Li, L.-J. Chen, H. Tan, C.-H. Wang, D.-X. Wang and H.-B. Yang, *Organometallics*, 2011, **30**, 5141–5146; (*e*) M. S. Inkpen, S. Scheerer, M. Linseis, A. J. P. White, R. F. Winter, T. Albrecht and N. J. Long, *Nat. Chem.*, 2016, **8**, 825–830; (*f*) A. Hildebrandt and H. Lang, *Organometallics*, 2013, **32**, 5640–5653; (*g*) U. Pfaff, G. Filipczyk, A. Hildebrandt, M. Korb and H. Lang, *Dalton Trans.*, 2014, **43**, 16310–16321; (*h*) Y. V. Zatsikha, C. D. Holstrom, K. Chanawanno, A. J. Osinski, C. J. Ziegler and V. N. Nemykin, *Inorg. Chem.*, 2017, **56**, 991–1000.

16 S. Bruña, A. M. González-Vadillo, D. Nieto, C. J. Pastor and I. Cuadrado, *Organometallics*, 2010, **29**, 2796–2807.

17 S. Bruña, J. Perles, D. Nieto, A. M. González-Vadillo and I. Cuadrado, *J. Organomet. Chem.*, 2014, **751**, 769–780.

18 See for example: (*a*) S. E. S. Martin and D. A. Watson, *J. Am. Chem. Soc.*, 2013, **135**, 13330–13333; (*b*) T. Moyori, T. Hayashi and A. Takasu, *J. Polym. Sci., Part A: Polym. Chem.*, 2013, **51**, 3516–3522; (*c*) C. Chen, S. Luo and R. F. Jordan, *J. Am. Chem. Soc.*, 2008, **130**, 12892–12893; (*d*) S. Luo and R. F. Jordan, *J. Am. Chem. Soc.*, 2006, **128**, 12072–12073.

19 (*a*) S. Santi, A. Bisello, R. Cardena and A. Donoli, *Dalton Trans.*, 2015, **44**, 5234–5257; (*b*) *Inorganic Electrochemistry*, ed. P. Zanello, F. Fabrizi de Biani and C. Nervi, Royal Society of Chemistry, Cambridge, 2nd edn, 2012; (*c*) S. Barlow and D. O'Hare, *Chem. Rev.*, 1997, **97**, 637–670; (*d*) D. Astruc, *Electron Transfer and Radical Processes in Transition-Metal Chemistry*, VCH, New York, 1995.

20 (*a*) W. E. Geiger and F. Barriére, *Acc. Chem. Res.*, 2010, **43**, 1030–1039; (*b*) F. Barriére and W. E. Geiger, *J. Am. Chem. Soc.*, 2006, **128**, 3980–3989; (*c*) A. Nadafy, T. T. Chin and W. E. Geiger, *Organometallics*, 2006, **25**, 1654–1663; (*d*) F. Barrière, N. Camire, W. E. Geiger, U. T. Mueller-Westerhoff and R. Sanders, *J. Am. Chem. Soc.*, 2002, **124**, 7262–7263; (*e*) R. J. LeSuer and W. E. Geiger, *Angew. Chem., Int. Ed.*, 2000, **39**, 248–250.

21 (*a*) D. A. Foucher, C. H. Honeyman, J. M. Nelson, B. Z. Tang and I. Manners, *Angew. Chem., Int. Ed. Engl.*, 1993, **32**, 1709–1711; (*b*) R. Rulkens, A. J. Lough, I. Manners, S. R. Lovelace, C. Grant and W. E. Geiger, *J. Am. Chem. Soc.*, 1996, **118**, 12683–12695; (*c*) D. E. Herbert, J. B. Gilroy, W. Y. Chan, L. Chabanne, A. Staubitz, A. J. Lough and I. Manners, *J. Am. Chem. Soc.*, 2009, **131**, 14958–14968.

22 (*a*) V. V. Dement'ev, F. Cervantes-Lee, L. Parkanyi, H. Sharma, K. H. Pannell, M. T. Nguyen and A. F. Diaz, *Organometallics*, 1993, **12**, 1983–1987; (*b*) M. T. Nguyen, A. F. Diaz, V. V. Dementiev and K. H. Pannell, *Chem. Mater.*, 1993, **5**, 1389–1394; (*c*) K. H. Pannell, V. V. Dementiev, H. Li, F. Cervantes-Lee, M. T. Nguyen and A. F. Diaz, *Organometallics*, 1994, **13**, 3644–3650.

23 When $[n\text{-}Bu_4N][PF_6]$ is used as the supporting electrolyte in the low polarity dichloromethane solvent, the strong ion pairing between the positively charged electrogenerated ferrocenium species and the $[PF_6]^-$ anion of the electrolyte, leave little or any electrostatic effect. See: A. K. Diallo, C. Absalon, J. Ruiz and D. Astruc, *J. Am. Chem. Soc.*, 2011, **133**, 629–641.

24 The value of K_c can be determined using the equation $K_c = \exp[F\Delta E_{1/2}/RT]$. See: D. E. Richardson and H. Taube, *Inorg. Chem.*, 1981, **20**, 1278–1285.

25 Both the $E_{1/2}$ and the splitting $\Delta E_{1/2}$ values are strongly dependent on the solvent and supporting electrolyte anion employed. See ref. 19 and references therein: (*a*) R. F. Winter, *Organometallics*, 2014, **33**, 4517–4536; (*b*) D. M. D'Alessandro and F. R. Keene, *Dalton Trans.*, 2004, 3950–3954.

26 M. B. Robin and P. Day, *Adv. Inorg. Chem. Radiochem.*, 1967, **10**, 247–422.

27 M. M. Montero-Campillo, S. Bruña, I. Cuadrado and O. Mó, *Comput. Theor. Chem.*, 2015, **1053**, 281–288.

28 This stripping-type behaviour was observed for the first time in poly(vinylferrocene). See for example: (*a*) J. B. Flanagan, S. Margel, A. J. Bard and F. C. Anson, *J. Am. Chem. Soc.*, 1978, **100**, 4248–4253; (*b*) A. Merz and A. J. Bard, *J. Am. Chem. Soc.*, 1978, **100**, 3222–3223.

29 U. Pfaff, A. Hildebrandt, D. Schaarschmidt, T. Rüffer, T. Hahn, J. Kortus and H. Lang, *Organometallics*, 2012, **31**, 6761–6771.

30 A. Nadafy and W. E. Geiger, *Organometallics*, 2008, **27**, 5624–5631.

31 J. Osteryoung and J. J. O'Dea, in *Electroanalytical Chemistry*, ed. A. J. Bard, Marcel Dekker, Inc., New York, 1986, vol. 14.

32 R. J. LeSuer, C. Buttolph and W. E. Geiger, *Anal. Chem.*, 2004, **76**, 6395–6401.

33 G. M. Sheldrick, *SADABS Version 2.03, Program for Empirical 951 Absorption Correction*, University of Göttingen, Germany, 1997–2001.

34 *SAINT+NT Version 6.04, SAX Area-Detector Integration Program*, Bruker Analytical X-ray Instruments, Madison, WI, 1997–2001.

35 *Bruker AXS SHELXTL Version 6.10, Structure Determination Package*, Bruker Analytical X-ray Instruments, Madison, WI, 2000.

36 G. M. Sheldrick, *Acta Crystallogr., Sect. A: Found. Crystallogr.*, 1990, **46**, 467–473.

37 G. M. Sheldrick, *SHELXL97, Program for Crystal Structure 960 Refinement*, Germany, 1997.

38 M. J. Frisch, *et al.*, *Gaussian09, Revision D.01*, Gaussian, Inc., Wallingford, 2009.
39 (*a*) J. P. Perdew, in *Electronic structure of solids*, ed. P. Ziesche and H. Eschrig, Akademie Verlag, Berlin, 1991; (*b*) A. D. Becke, *Phys. Rev. A*, 1988, **38**, 3098.
40 E. R. Johnson, S. Keinan, P. Mori-Sánchez, J. Contreras-García, A. J. Cohen and W. Yang, *J. Am. Chem. Soc.*, 2010, **132**, 6498–6506.
41 R. F. W. Bader, *Atoms in molecules: a quantum theory*, Clarendon, Oxford, 1990.